# Experimental Investigation on the Unsteady Surface Pressure Fluctuation Patterns over an Airfoil

Alper Celik*, Luke Bowen† and Mahdi Azarpeyvand ‡
*Swansea University, Swansea,UK, SA1 8EN*
*University of Bristol, Bristol,UK, BS8 1TR*

**This article presents a comprehensive mapping of wall pressure fluctuations over an airfoil under three different inflow conditions to shed light on some basic assumptions taken granted for the recent aeroacoustic and aerodynamics experimental studies and in the noise prediction models. Unsteady and steady pressure measurements were performed over a heavily instrumented airfoil which was exposed to smooth inflow, grid generated turbulent inflow, and a smooth inflow with a tripping tape over the airfoil to explore the unsteady response of the airfoil for a broad range of angles of attack,** $0^\circ \leq \alpha \leq 20^\circ$**. The results are presented in terms of non-dimensional pressure coefficient, root mean square non-dimensional pressure coefficient, frequency-energy content pattern map at isolated frequencies for the entire airfoil, and spectra of frequency-energy content at selected transducer locations. The results show that the unsteady airfoil response patterns for the tripped boundary layer and turbulence ingestion cases show a dramatic difference compared to the airfoil response patterns of the smooth inflow conditions. The response patterns differ across angles of attack, frequency, and between both sides of the airfoil. The results suggest a three region pattern for smooth inflow case, a two region pattern for tripped boundary layer case, and a two region pattern for the turbulence ingestion case. Moreover, the results indicate that the presence of tripping may provide a flow with necessary statistical characteristics for the experimental rigs representing the full-scale application; however, it may misrepresent the frequency-dependent nature of the boundary layer.**

## I. Nomenclature

$c$ = Chord [m]

$C_p$ = Non-dimensionalized coefficient of pressure [-]

$C_{p,rms}$ = Non-dimensionalized root mean square coefficient of pressure [-]

*Lecturer, Department of Aerospace Engineering , alper.celik@swansea.ac.uk
†PhD. Student, Mechanical Engineering, luke.bowen@bristol.ac.uk
‡Professor of Aerodynamics and Aeroacoustics, Mechanical Engineering, m.azarpeyvand@bristol.ac.uk

$d$ = Diameter [mm]

$f$ = Frequency [Hz]

$M$ = Mesh size [mm]

$p$ = Pressure [Pa]

$p'$ = Pressure fluctuation [Pa]

$p_o$ = Reference pressure $2 \times 10^{-5}$ [Pa]

$PSD$ = Power spectral density [dB/Hz]

$Re$ = Reynolds number [-]

$t$ = Thickness [mm]

$TI$ = Turbulence intensity [%]

$U$ = Free-stream velocity [m/s]

$kc$ = Helmholtz number [-]

$\alpha$ = Angle of attack [°]

$\Lambda$ = Integral Length Scale [mm]

$\phi_{pp}$ = Power spectral density of the pressure fluctuations [dB/Hz]

## II. Introduction

The unsteady loading generated over solid surfaces immersed in a flow is of great interest as it is ubiquitous for many applications, including aircraft, engines, turbo-machinery, and wind turbines. A sound and fundamental understanding of the unsteady loading on airfoils at various operating and flow conditions will help us improve the existing prediction tools for a range of applications, including aeroelasticity, aerodynamics, and aeroacoustics. A grasp of the underpinning physics may, in turn, provide adequate tools to decrease the environmental impact of the relevant technologies [1, 2]. This can also help us develop more bespoke and effective gust interaction mitigation tools, effective suppression of Tollmien-Schlichting (T-S) instabilities for blades operating at low Reynolds numbers, development of blade geometrical features for suppression of loading over the trailing edge area and thus trailing edge noise. The unsteady surface pressure fluctuations over an airfoil arise from complex interactions between the inflow and the boundary layer over the airfoil. Unsteady aspects of the inflow such as gusts or turbulence, and the instabilities in the boundary layer, such as transition, contribute to the complexity of the problem. The undesirable vibration due to the unsteady pressure fluctuations (lift) may lead to structural problems [3–6], as well as radiated noise [7–9]. The unsteady loading and the lift generated by unsteady loading has been first addressed by Theodorsen [10] , which is followed by works of von Karman and Sears [11], Sears [8], and Atassi [12].

The unsteady loading analysis has traditionally focused on either the leading edge or trailing edge areas, depending on

the application, ignoring the effects of boundary layer evolution over the airfoil and the importance of flow development. A sound understanding of the unsteady response of the wing is of crucial importance for aeroacoustics. The two main categories of aeroacoustic studies related to the lifting and non-lifting airfoil geometries are the airfoil self-noise and the interaction noise. As discussed in detail by Brooks *et al.* [13], self-noise involves trailing edge turbulent boundary layer noise, stall noise, separation noise, laminar boundary layer-vortex shedding noise, and tip vortex noise. Interaction noise arises from the interaction of incoming turbulent structures or gusts with the airfoil's leading edge. Outlet vane guides (OGV) in modern turbofan engines and wind turbines (interaction with the highly turbulent air) are two of the many examples that interaction noise being of concern. There is a broad range of studies addressing the prediction methods for aerodynamically generated noise (for both trailing edge and leading edge interaction noise), which requires flow domain information, i,e., either two point velocity correlations in the flow field or unsteady surface pressure fluctuations over the airfoil [9, 14–17]. As manifested in the classical work of Curle [7], the far-field noise radiated from an airfoil immersed in a turbulent flow can be predicted with the knowledge of unsteady surface pressure fluctuations experienced by the airfoil, or unsteady lift as depicted by Howe [18], under the assumption of sufficiently small Mach number and acoustically compactness. Despite the need for extensive data sets for realistic predictions, the literature on the methods that require unsteady surface pressure fluctuations as input is quite limited. Studies such as Orlemans and Miglore [19], Moreau et al. [20], McKeough [21], Mish and Devenport [22, 23], and Davenport [24] conducted experimental investigations on various airfoil geometries under realistic conditions such as non-zero angles of attack and airfoils immersed in grid generated turbulence. Stall and separation noise is also a crucial aspect of the airfoil self-noise. However, since most of the designs are for attached flow, the studies on separation and stall noise remained rather limited. Brooks et al. [13] was one of the pioneering works to address separation and stall noise, where a semi-empirical noise prediction method was also proposed. With the advancement in the wind turbine industry, studies on stall and separation noise also accelerated.Moreau et al. [25], Bertagnolio et al. [26], Mayer et al. [27], and Zang et al. [28] performed experimental studies to shed light on the parameters affecting stall noise and the underpinning physical mechanisms. The leading edge interaction noise methods in the literature are based on Amiet [9] and addressed less [29–32] compared to the trailing edge noise problem. Theoretical models such as Amiet and Sears [33], Atassi [34], Glegg [35] among others are based on the modeling of turbulence as a gust. However, any prediction model for the unsteady lift or unsteady surface pressure fluctuations inherently includes many assumptions which would not reflect all the varieties and uncertainties in a real life application.

Obtaining surface pressure fluctuations to improve prediction models to help early design process through experiments has its own limitations and challenges. The experimental studies were primarily conducted in wind tunnels with size limitations, where the transition from laminar flow regime to turbulent flow regime is unlikely to occur due to the size of the test models. In order to achieve a turbulent flow over the airfoil, or at least over the trailing edge, and to mimic the conditions at high Reynolds number flow that the actual wings experience, a tripping tape is utilized to force an early

(forced) transition to the turbulent regime over the airfoils in experiments [36–40]. Despite its utilization in almost all experiments, the number of investigations addressing the effect on mean quantities is limited [41–43] and frequency dependent effect does not exist. The tripping is specifically crucial in aeroacoustic measurements, where the instabilities prior to transition lead to Tollmien-Schlichting (T-S) waves. T-S waves generate a high-amplitude tonal noise that contaminates or dominates the other noise sources. Although the tripping is used as a standard technique to achieve turbulent flow over an airfoil, the rich nature of the transition, and the chordwise history of the unsteady response over the airfoil are quite neglected in the literature. Moreover, the effect of the tripping on the unsteady loading on the airfoil has also often been shadowed as long as the statistical quantities are matched. The aeroacoustic prediction methods also neglect the asymmetrical conditions that may arise at non-zero angles of attack, which are inevitable in realistic scenarios.

This study aims at understanding and reporting the effect of smooth inflow, smooth inflow with tripped boundary layer and turbulent inflows on unsteady pressure fluctuations and their corresponding reflections on frequency-dependent energy, i.e., airfoil response, over a broad range of angles of attack over the entire airfoil surface. Much of this study is focused on airfoil response patterns qualitatively rather than focusing on the direct aeroacoustic or aerodynamic interpretation. The study also aims to provide comprehensive experimental data across the entire chord of a NACA0012 airfoil to be used as an input for both aeroacoustic and aerodynamic prediction and validation models in the literature. The paper is organized as follows. Section III introduces the experimental set-up, airfoil model, and the instrumentation with brief details of post-processing techniques. Section IV provides a detailed discussion on the results in two sub-sections. Section IV.A presents the results of the steady measurements. The detailed mapping of the surface pressure fluctuations is presented in Sec. IV.B. Lastly, the paper is concluded in Sec. V with some future remarks.

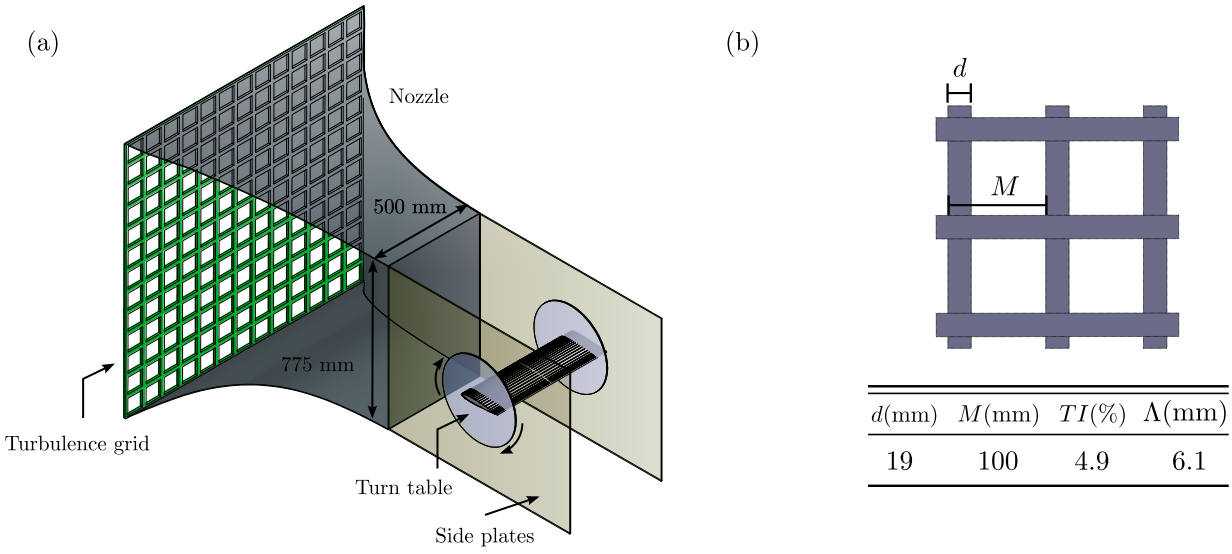


| $d$(mm) | $M$(mm) | $TI$(%) | $\Lambda$(mm) |
|---|---|---|---|
| 19 | 100 | 4.9 | 6.1 |

**Fig. 1 Schematics of the experimental rig (a) airfoil, side plates and the turbulence grid, (b) geometric properties of the grid and the associated flow quantities.**

## III. Experimental Set-up

The experiments were performed at the University of Bristol Aeroacoustic Facility, which is a closed-circuit, open-jet anechoic wind tunnel, shown in Fig. 1. The chamber is anechoic down to 160 Hz with physical dimensions of 6.7 m x 4.0 m x 3.3 m. The nozzle had a contraction ratio of 8.4:1 and had dimensions of 500 mm in width and 775 mm in length, which allows a steady operation from 5 m/s to 45 m/s, and a normal turbulence intensity levels below 0.2% [44].

A highly instrumented NACA (National Advisory Committee for Aeronautics) 0012 airfoil with pressure taps for both steady and unsteady surface pressure was used in the study in order to capture the aerodynamic and aeroacoustic phenomena. The NACA 0012 airfoil was designed, manufactured and instrumented in-house at the University of Bristol. The airfoil was manufactured using rapid prototyping methods to enable intricate internal and external details for heavy instrumentation. An Ultimaker S2 3D printer, which utilized Polylactic acid (PLA), was used to manufacture the airfoil with a chord of 0.2 m and a span of 0.6 m. For maximum resolution and accuracy, the step height was set to 0.06 mm and the nozzle thickness was 0.2 mm. All gaps were smoothed with resin and the airfoil surface was post-processed using sand paper. It was sanded in increments up to 600 grit, which results in an approximate surface roughness of $0.13 \times 10^{-6}$. To ensure the shape was not lost due to sanding, a sanding block with the exact profile of the NACA 0012 airfoil was used. For instrumentation, brass tubes were installed into recesses over the airfoil, using a two part epoxy resin and smoothed into the surface. Demonstrated in Fig. 2, instrumentation included 56 pressure taps for the measurement of the hydrodynamic field around the airfoil, and 56 taps for unsteady surface pressure fluctuation measurement. For both the steady pressure taps and the unsteady pressure taps 0.4 mm pinholes were drilled on the brass tubes to avoid pressure attenuation at high frequencies. Steady pressure measurements were performed using two 32-channel Chell MicroDaq Smart Pressure Scanners. The steady pressure data were collected for 16s, with a sampling frequency of 1000 Hz. The propagated uncertainty value was 2.5% for the lowest measured pressure values.

The unsteady surface pressure measurements were performed remotely by using Panasonic WM-61A microphones. Polyurethane tubes with a wall thickness of 1.4 mm were used to connect the brass tubes to the microphone assembly (microphone and microphone holder), as illustrated in Fig. 1(c). In addition, one end of the microphone holder is connected to a 2 m polyurethane tubing, utilized as an anechoic termination to avoid noise contamination from high-frequency noise reflections. Each microphone was calibrated in situ for both magnitude and phase, referenced to a single GRAS 40PL microphone, calibrated using a GRAS 42AA pistonphone calibrator. The in situ calibration provided a transfer function for calibration that accounted for connection tubes' effects, damping at high frequencies and other sources that may arise from the rig assembly. The data were acquired using National Instrument PXIe-4499 module and were sampled at $2^{16}$ Hz for a duration of 16 seconds. The power spectrum (power spectral density) of the surface pressure fluctuations was estimated by using the Welch method [45], where the data from the transducers are segmented for 32 equal lengths with 50% overlap and windowed by the Hamming function, and the resulting spectrum had a frequency resolution of $\Delta f$ =2 Hz. The surface pressure data obtained gives an absolute uncertainty of ±0.05 dB

with a 95% of confidence level.

The experiments were conducted at a free stream velocity of $U$ = 20 m/s which corresponds to a chord based Reynolds number $Re$ = 2.6 x $10^5$. The measurement were performed under three different conditions, i.e., smooth inflow, tripped boundary layer and turbulent inflow. For smooth inflow conditions, the tunnel was operated under steady conditions, which leads to a turbulence intensity of 0.2%. For tripped boundary layer condition, the flow over the airfoil was tripped at 20% of the chord via a 60° zig-zag turbulator tape on both sides of the wing to ensure turbulent boundary layer. For the turbulent inflow case, a passive grid was located in the nozzle contraction as illustrated in Fig.1, which generates a turbulence intensity of $TI$ = 4.9% and flow structures with an integral length scale of $\Lambda$ = 6.1 mm at $x'/c$ = 0. The details of the generated grid turbulence can be accessed in [46]. In order to enable a comprehensive assessment of the effect of inflow conditions at a broad range of operating conditions, the experiments were conducted for angles of attack spanning −6° to 20° with and increment of 2°.

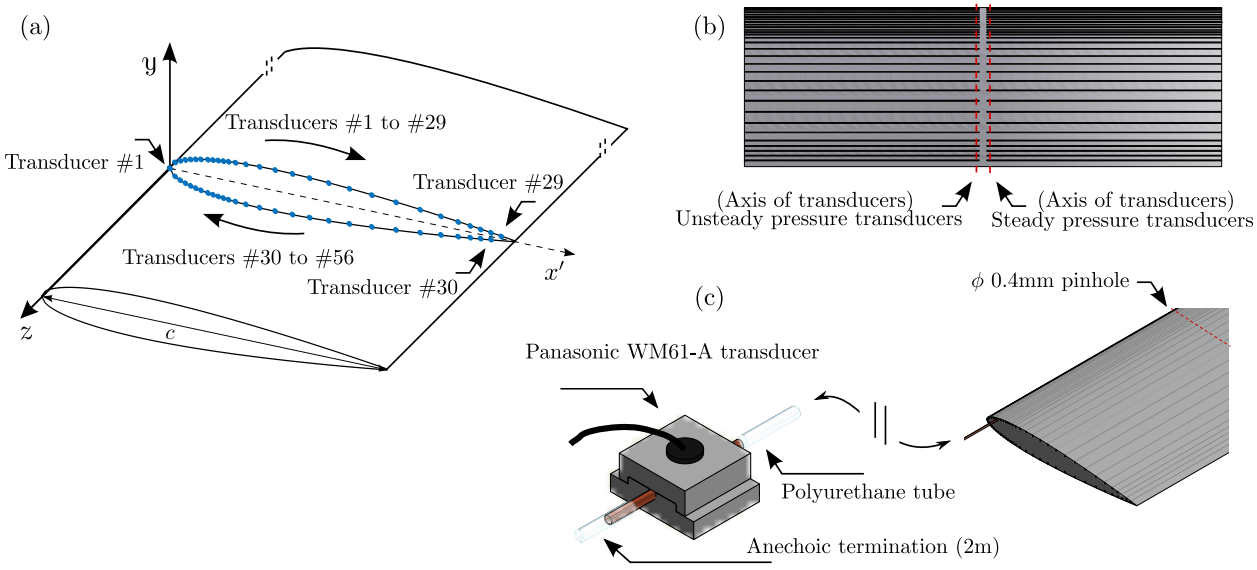


**Fig. 2 Schematics of the NACA0012 airfoil (a) streamwise locations for both the unsteady and steady pressure transducers, (b) axis of transducers, (c) details of remote sensing setup .**

## IV. Results & Discussion

In this section, the results of the experiments are presented in terms of steady (static) and unsteady (dynamics) aspects to explore the effect of three different flow conditions over a broad range of angles of attack. The results are presented in terms of non-dimensional pressure coefficient, root mean square non-dimensional pressure coefficient, frequency-energy content pattern map at isolated frequencies for the entire airfoil, and spectra of frequency-energy content at selected transducer locations.

**Table 1 Streamwise locations of the unsteady surface pressure transducers. All transducers are located at a spanwise distance of $z/c = 0.05$. (Steady pressure transducers are located at $z/c = -0.05$ for the same streamwise locations. )**

| Transducer | $x'/c(\%)$ | Transducer | $x'/c(\%)$ | Transducer | $x'/c(\%)$ |
|---|---|---|---|---|---|
| T1 | 0 | T11, T47 | 0.15 | T21, T37 | 0.58 |
| T2, T56 | 0.015 | T12, T46 | 0.17 | T22, T36 | 0.65 |
| T3, T55 | 0.030 | T13, T45 | 0.19 | T23, T35 | 0.725 |
| T4, T54 | 0.045 | T14, T44 | 0.22 | T24, T34 | 0.78 |
| T5, T53 | 0.060 | T15, T43 | 0.26 | T25, T33 | 0.83 |
| T6, T52 | 0.075 | T16, T42 | 0.30 | T26, T32 | 0.87 |
| T7, T51 | 0.090 | T17, T41 | 0.35 | T27, T31 | 0.90 |
| T8, T50 | 0.11 | T18, T40 | 0.40 | T28, T30 | 0.93 |
| T9, T49 | 0.12 | T19, T39 | 0.46 | T29 | 0.96 |
| T10, T48 | 0.14 | T20, T38 | 0.52 | | |

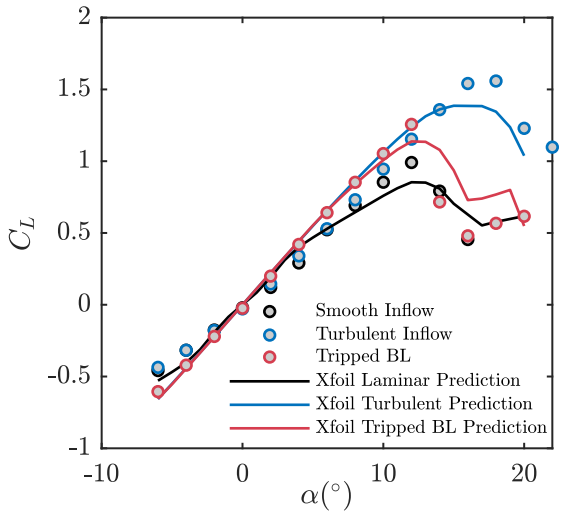


**Fig. 3 Comparison of mean lift coefficient ($C_L$) as function of angle of attack, $0^\circ \leq \alpha \leq 20^\circ$, under three different flow conditions. Xfoil predictions are presented for comparison.**

### A. Steady pressure measurements

The 3-D printed airfoil was validated to ensure it accurately represented the geometry, and the employment of sensors was non-intrusive. To check this, all cases, i.e., the smooth inflow case, tripped boundary layer case, and the turbulent inflow cases, were considered and tested and compared to XFoil predictions. The inflow turbulence level is simulated in XFoil by using the "NCrit" parameter, which controls the trigger of the natural transition. As the aeroacoustic wind tunnel is an open jet type wind tunnel, the geometric angle of attack is not the true angle of attack experienced by the airfoil due to the deflection of the jet and a correction was required. The angle of attack correction is

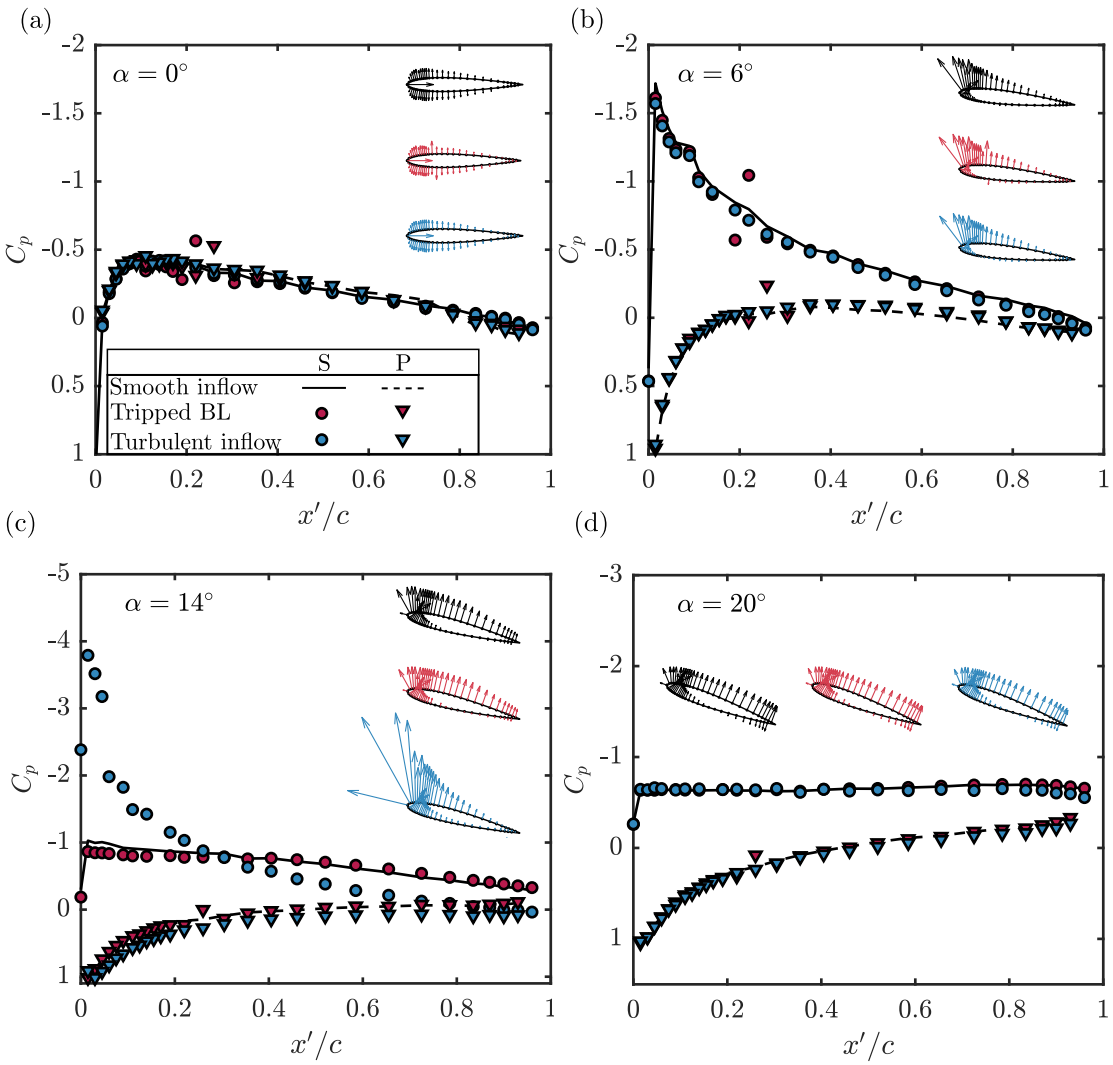


**Fig. 4 Comparison of $C_p$ distribution for smooth inflow, tripped boundary layer, and turbulent inflow conditions at angles of attack $\alpha = 0°, 6°, 14°$ and $20°$. (S and P in the legend refer to airfoil suction and pressure sides, respectively)**

achieved by validating the measured experimental pressure distribution with a computed pressure distribution from XFoil. The results for the pressure distribution is not shown here for brevity. The maximum deviation from actual angle was 3°, and was just before the separation started, i.e, the end of the linear region for $C_L$ curve, as presented in Fig. 3. Hereafter, the results are presented in terms of geometrical angles of attack.

Following the validation of the results, the characterization of the mean pressure field was performed by comparing the non-dimensional pressure coefficient $C_p$ and root-mean-square (rms) pressure coefficient, $C_{p,rms}$, for a broad range of angles of attack. For brevity, the results are presented for selected cases, i.e., $\alpha = 0°, 6°, 14°$ and $20°$. Figure 4 presents the results of non-dimensional pressure coefficient distribution, $C_p$, over the entire airfoil (for both suction and pressure side) at the angles of attack of $\alpha = 0°, 6°,$ $14°$ and $\alpha = 20°$ for all inflow conditions. Moreover, a visual

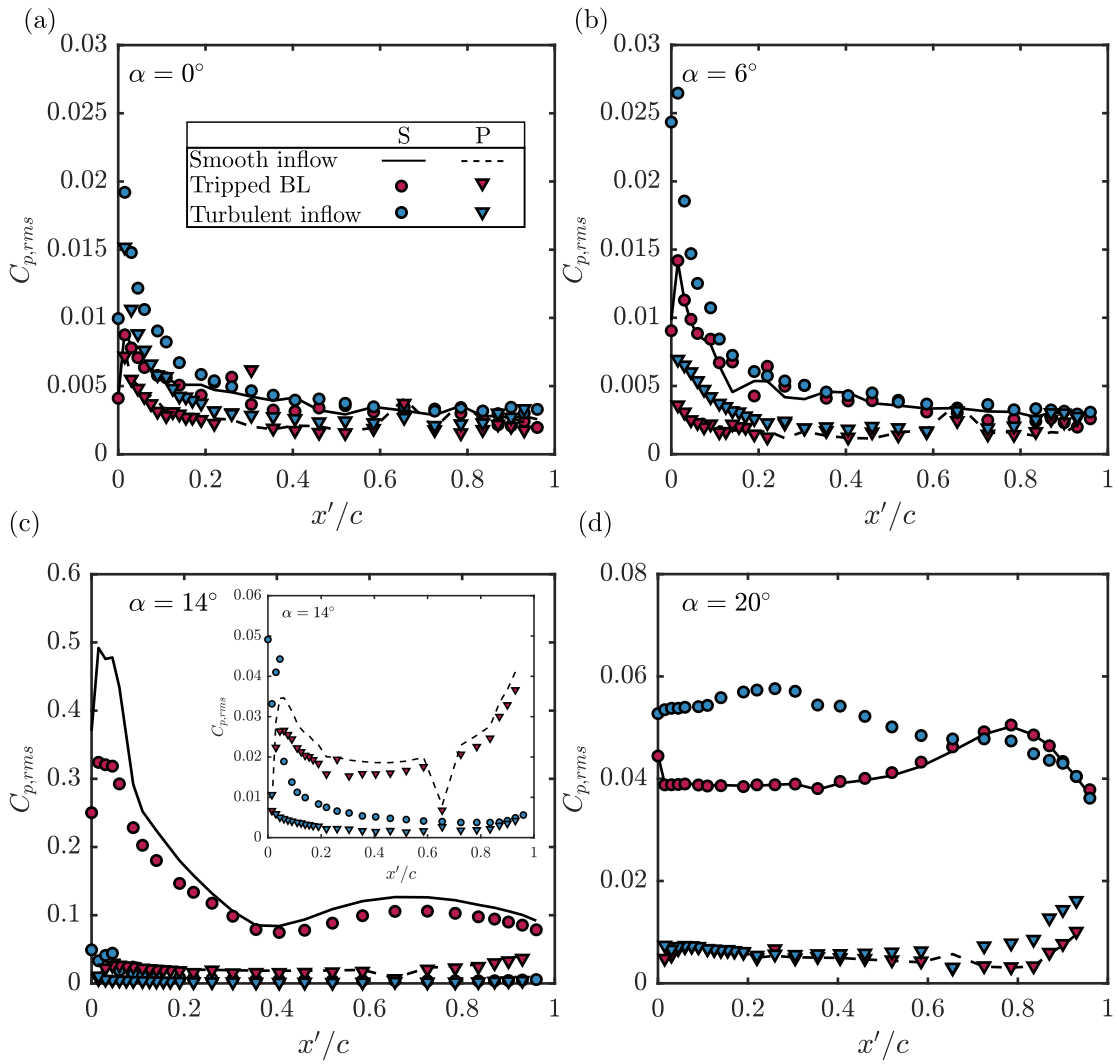


**Fig. 5 Comparison of $C_{prms}$ distribution for Comparison of $C_p$ distribution smooth inflow, tripped boundary layer, and turbulent inflow conditions at angles of attack $\alpha = 0°, 6°, 14°$ and $20°$. (S and P in the legend refer to airfoil suction and pressure sides, respectively)**

representation of the corresponding $C_p$ on actual airfoil geometry is illustrated for each case to ease the interpretation of the data.

The pressure distribution results at the angle of attack $\alpha = 0°$ display a symmetric distribution on both sides of the airfoil for all cases, as expected. The $C_p$ curves are in agreement at $\alpha = 6°$ as well, which indicates that the flow conditions, i.e., smooth inflow, turbulent inflow, and tripped boundary layer, do not have a significant effect on the $C_p$ distribution and magnitude. At a sufficiently higher angle of attack, $\alpha = 14°$, the $C_p$ curves, associated with smooth inflow and tripped boundary layer cases show a similar trend, with an indication of flow separation, as the reduced and relatively flattened curves suggest. However, the results for the turbulent inflow case display significantly different behavior, with drastically elevated $C_p$ magnitudes, suggesting an attached flow as opposed to other cases. The increased

$C_p$ values also indicates elevated levels of lift force generation for this case. At $\alpha = 20°$, all $C_p$ curves collapse to a single flat line over the suction side, indicative of stalled airfoil for all cases.

To gain a better understanding of the effect of the inflow conditions at different angles of attack on the mean features of the airfoil response, the root-mean-square of the pressure coefficient, $C_{p,rms}$ is presented in Fig. 5. The $C_{p,rms}$ distribution may be interpreted as a footprint of turbulence levels over the airfoil. The figure is constructed similarly with Fig. 4. For $\alpha = 0°$, the results of the smooth inflow and tripped boundary layer cases display similar levels of fluctuation, whereas the turbulent inflow generates a pronounced increase of $C_{p,rms}$ around the leading edge. Recall that the $C_p$ distribution, presented in Fig. 4, was similar for all inflow conditions. It is also worth mentioning that $C_{p,rms}$ distribution on the suction side and the pressure side of the airfoil do not exhibit an exact match, as $C_p$ distributions do. These observations are valid for the results at $\alpha = 6°$, with elevated magnitudes at the suction side and lower magnitudes on the pressure side. At $\alpha = 14°$, where the $C_p$ distributions indicate flow separation for smooth inflow case and tripped boundary layer case, a significant increase of fluctuations are evident at the leading edge. On the contrary, low levels of $C_{p.rms}$ persists for the turbulent inflow case over the entire airfoil. Lastly, at $\alpha = 20°$, where the airfoil is stalled for all cases, the results show higher levels of fluctuations compared to the results at $\alpha = 0°$ and $\alpha = 6°$ but lower than $\alpha = 14°$ on the suction side. Moreover, the $C_{p,rms}$ values for turbulent inflow cases are substantially higher than the results of other cases. It is worth noting that the $C_{p,rms}$ distribution on the suction side show a slight increase towards the trailing edge for the smooth inflow and tripped boundary layer case, whereas a gradual decrease after $x'/c = 0.2$ is evident for the turbulent inflow case results.

### B. Unsteady response pattern over NACA0012 airfoil

This part of the paper is dedicated to exploring the unsteady nature of the pressure response over the airfoil at different inflow conditions at a broad range of angles of attack. The results aim at exploring the history of the unsteady surface pressure fluctuations over the entire airfoil and the effect of tripping on the surface pressure patterns, which is mostly neglected in the literature. Turbulence ingestion results are also presented to enrich and complement the discussions. Results from a broad range of conditions under investigation may serve as valuable data set for numerical models and prediction methods.

Figure 6 presents the unsteady energy content of the wall pressure fluctuations (response) over a NACA0012 profile at $\alpha = 0°$ under three different flow conditions, i.e., smooth inflow, turbulent inflow (under grid generated turbulence), and tripped flow at the leading edge. The results are presented for a broad range of isolated frequencies, presented in terms of non-dimensional Helmholtz number, $kc = 2\pi fc/c_o$, where $f$ and $c_o$ refer to frequency and speed of sound, respectively. The results are presented for $kc = 0.73$, 2.21, 3.70, 5.54, 7.40, and 11.08, corresponding to $f = 200$, 600, 1000, 1500, 2000 and 3000 Hz. A reference arrow is placed on the corner of the figures, which represents 60 dB/Hz. The complete energy spectra at selected stream-wise locations are presented in Fig. 7 to complement the

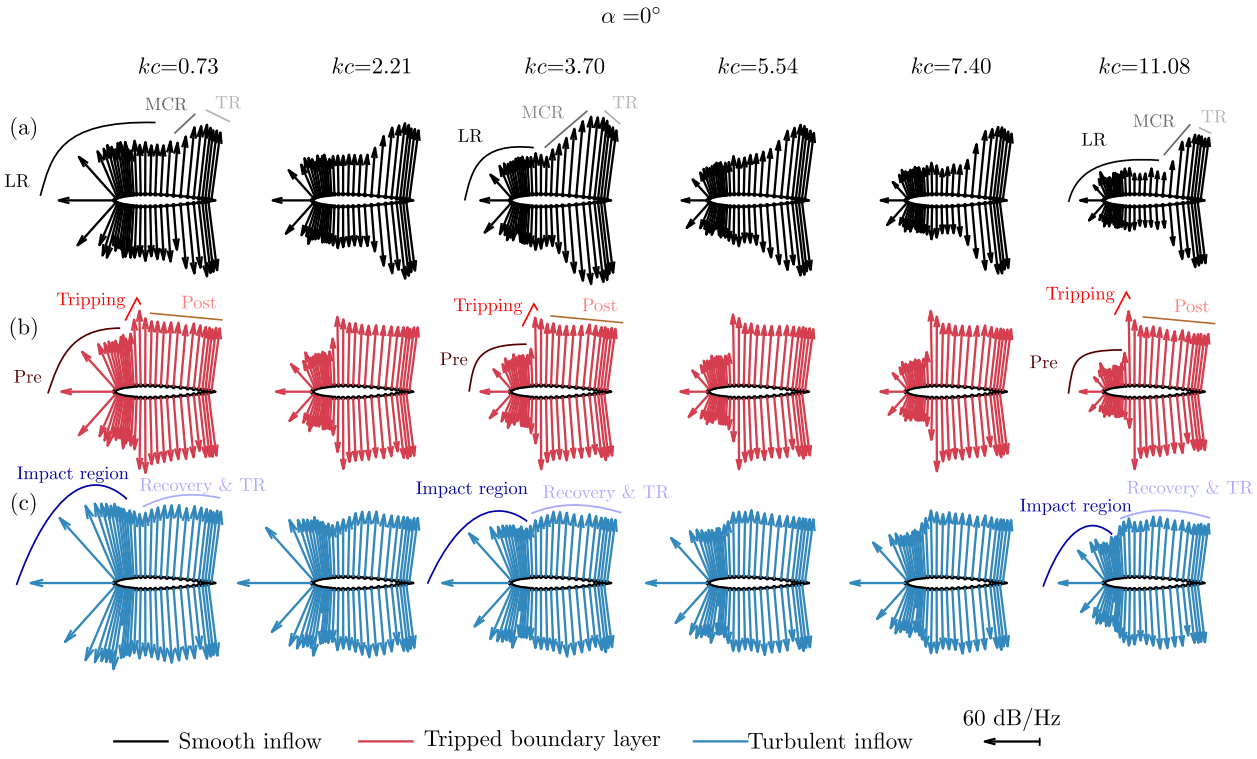


**Fig. 6 Comparison of unsteady airfoil response at angles of attack $\alpha = 0°$ for $0.73 \leq kc \leq 11.08$ under various flow conditions: (a) smooth inflow, (b) tripped boundary layer, (c) grid turbulence.**

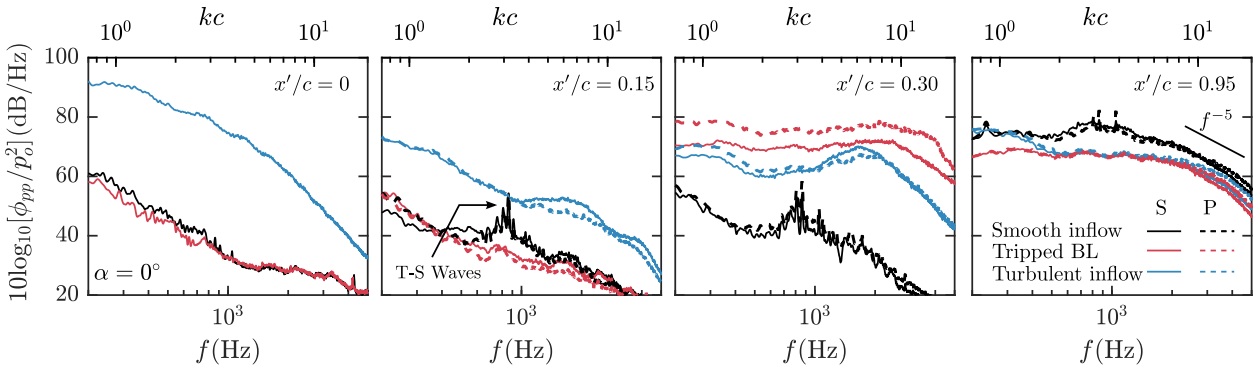


**Fig. 7 Energy spectra of the pressure fluctuations (response) for the transducers located at $x'/c = 0$, 0.15, 0.3 and 0.95 on both the pressure and suction side of the wing for different flow conditions at $\alpha = 0°$.**

interpretation of the results.

At first glance, Fig. 6 reveal the rich nature of the flow interaction with some distinct features across different inflow conditions. The unsteady loading response (energy content) over the airfoil for smooth inflow case can be described by partitioning the region over the airfoil in three regions, namely, leading edge region (LR), mid-chord transition region (MCR) and trailing edge region (TR). For low $kc$ values, LR and TR dominate the airfoil response, where LR stretches over most of the airfoil. At mid $kc$ values, both LR, MCR, and TR exists strongly. Conversely, for the tripped boundary layer case, the response on the airfoil has only two regions, namely pre-transition and post-transition regions. The

sharp transition to a highly energetic response after the tripping dominates the rest of the flow over the airfoil. For the turbulence interaction case, two regions are apparent from the response patterns, a leading edge region, where the impact of turbulence ingestion is strongly felt and slowly decays toward mid-chord region, and a second region, with a transition to a more stable flat response until the trailing edge. To ease the interpretation, signaling lines are placed in the figure.

Focusing on the results for each flow condition may reveal more information on the airfoil response for a broad range of $kc$ values. The smooth inflow results in Fig. 6(a) at the lowest frequency, which corresponds to $kc = 0.73$, the airfoil response at the leading edge is relatively uniform and extends over the airfoil (LR), which is followed by a short, gradually increasing response region (MCR) just before the trailing edge. As the frequency increases, $kc = 2.21$ ($f = 600$ Hz), the LR pattern remains similar with a decrease in the response magnitude compared to the results at $kc = 0.73$, yet persists a uniform behavior until $x'/c = 0.5$. Furthermore, the extent of MCR increased toward the leading edge. A further increase in the frequency to $kc = 3.70$ is accompanied by a decrease in the airfoil response magnitude around the leading edge. The significantly reduced extent of LR is accompanied by a dominant MCR. The results at higher frequencies exhibit a gradual decrease in the magnitude of the response over the entire airfoil and a similar response pattern to lower $kc$ values with a dominant LR region, followed by a short MCR and TR. At $kc = 11.08$, the LR stretches until the trailing edge with a very short MCR. However, the response over the airfoil is dominated by the trailing edge region since the response magnitude for LR and MCR is significantly lower than the trailing edge results. The results suggest an evolution of airfoil response from a more uniform distribution at low Helmholtz numbers (low frequencies) to trailing edge dominant characteristics at high Helmholtz numbers for the smooth inflow case. These observations are consistent with Garcia-Sagrado and Hynes [47].

In contrast to observations for smooth inflow case, the results for the tripped boundary layer case, Fig. 6(b), display mostly uniform airfoil response over the entire chord, except the leading edge (pre-transition region), across the entire frequency range, $0.73 \leq kc \leq 11.08$. The low energy level at the leading edge region is similar to the results of the smooth inflow case until the tripping region. Beyond the tripping point (post-transition region), a substantial increase in energy is evident. It is worth noting that the transition takes place sharper at higher $kc$ values, compared to the gradual change of the response at low $kc$ values. Moreover, the response magnitude decreases as the $kc$ increases in the pre-transition region. Apart from increasing the overall energy content on the rest of the airfoil, the tripping has an immediate effect at its proximity, which becomes more apparent at higher frequencies, and slowly decays toward the mid-chord region across all $kc$ values. Considering the far-field noise prediction methods in conjunction with the aforementioned observations the following observation can be deduced. Unlike the smooth inflow case, the tripped cases have shown that the unsteady loading can be significantly different to the smooth flow case as the boundary layer evolution changes significantly. Such forced transition can lead to significantly spatial/temporal characteristics of the BL over the mid-chord and TE area.These interpretations are corroborated with the following results at higher angles of attack.

When the airfoil encounters a turbulent inflow, Fig. 6(c), the magnitude of the unsteady response exhibits a drastic increase at the leading edge until $x'/c = 0.15$ at the lowest frequency presented, i.e., $kc = 0.73$, compared to the results of smooth inflow and tripped flow conditions. The unsteady response at the leading edge deserves further attention. Firstly, the response magnitude at the leading edge, the impact generated by turbulence interaction, gradually decreases as the $kc$ increases. Secondly, at low $kc$ values, $kc \leq 3.70$, the elevated response at the leading edge decays toward the mid-chord region, where it reaches a minimum. Subsequently, a short transition region is evident, evolving into a flat-like pattern, similar to the results of tripped boundary layer case.

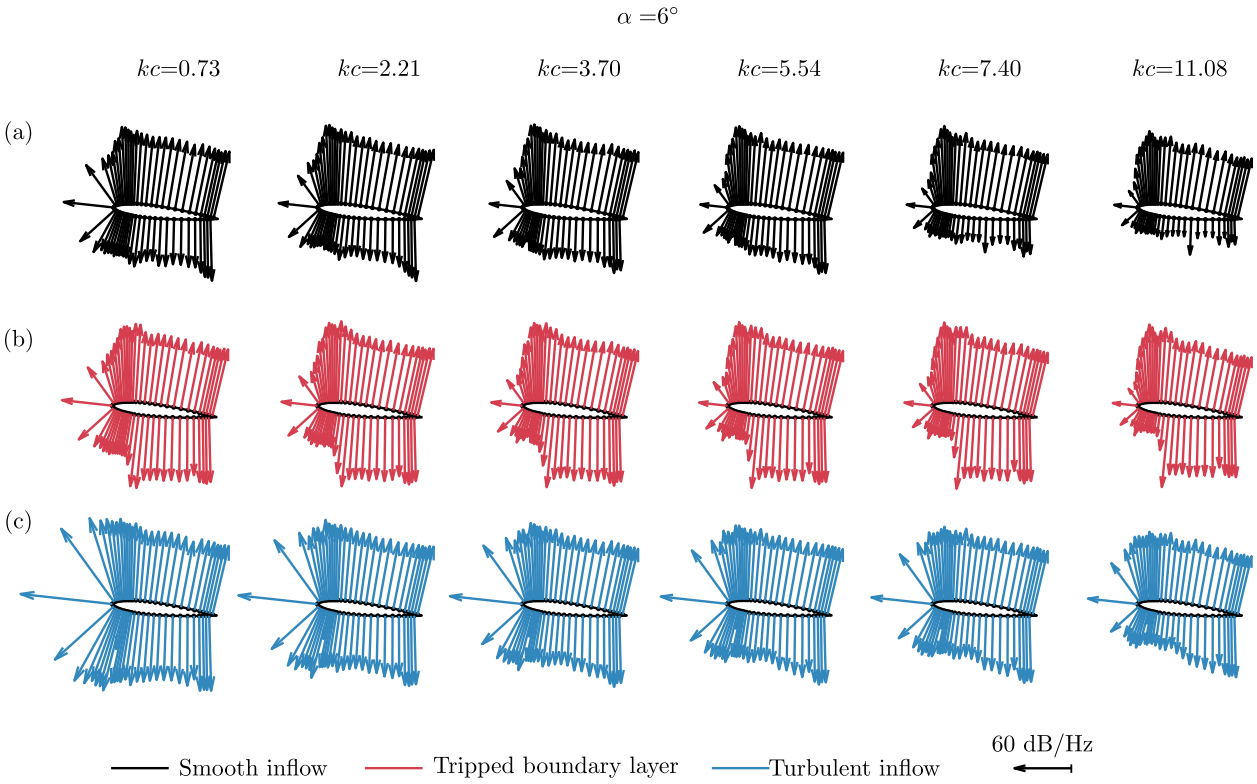


**Fig. 8 Comparison of unsteady airfoil response at angles of attack $\alpha = 6°$ for $0.73 \leq kc \leq 11.08$ under various flow conditions: (a) smooth inflow, (b) tripped boundary layer, (c) grid turbulence.**

It is also intriguing to observe the unsteady loading response over the entire frequency range for selected transducers, as presented in Fig.7. At the stagnation point, $x'/c = 0$, turbulent inflow conditions lead to significantly elevated energy levels compared to the results of the smooth inflow and tripped boundary layer case. At $x'/c = 0.15$, the footprints of T-S (Tollmien-Schlichting) waves are evident with an apparent pattern of discrete peaks of equi-distanced frequencies with a central frequency of $f = 862$ Hz on both sides of the airfoil for the smooth inflow conditions. These peaks are also evident at the far-field noise measurements, which are not shown here for brevity and are indicators of T-S instabilities in the literature [48, 49]. Further downstream, the energy spectra for the tripped boundary layer case exhibit a typical developing flow behavior. The response spectra for the turbulent inflow case, however, shows an unusual wavy

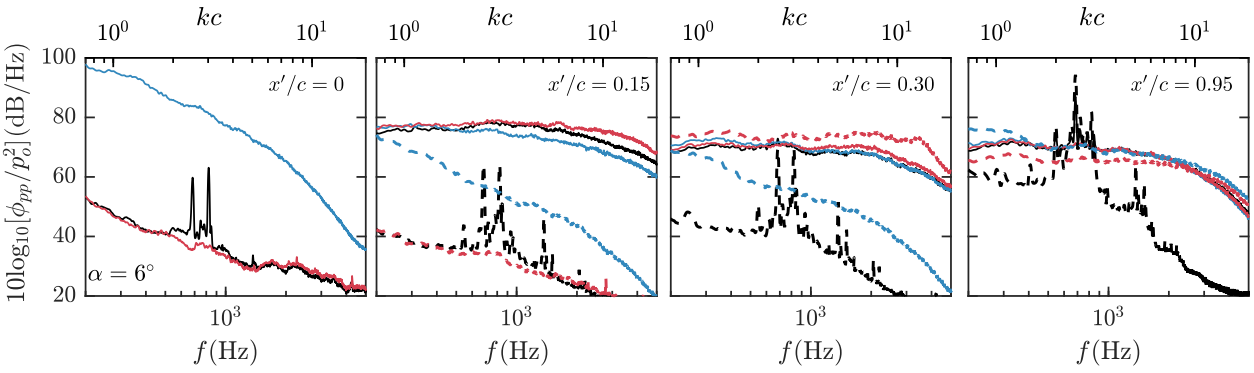


**Fig. 9 Energy spectra of the pressure fluctuations (response) for the transducers located at $x'/c = 0$, 0.15, 0.3 and 0.95 on both the pressure and suction side of the wing for different flow conditions at $\alpha = 6°$**

pattern, which might be due to complex nature of the interaction between oncoming structures, airfoil and developing boundary layer. At the trailing edge, the energy spectra display a similar behavior for all cases, with slightly higher magnitudes for the results of the smooth inflow conditions, which also displays reminiscent of T-S waves. It is worth mentioning that at this location, the energy scales with $f^{-5}$ for all cases, which is typical for 2D turbulent boundary layers, as observed in the literature [47, 50–53] at mid-frequency range ($3.70 \leq kc \leq 7.40$). Another interesting result to highlight is that the presence of T-S waves has a very limited effect on the response pattern over the airfoil. Although not shown for brevity, this observation is valid across all frequencies and angles of attack where T-S waves are present.

At a moderate angle of attack, $\alpha = 6°$, the symmetrical airfoil response observed at $\alpha = 0°$ changes into an asymmetrical response for all cases over the entire range of frequencies. Figures 8 and 9 present the airfoil response for isolated frequencies over the airfoil and entire frequency range for selected transducers, respectively. The overall behavior of the response patterns can be summarized as follows. For the smooth inflow case, the three region behavior persists with a significant change in the pattern on both sides of the airfoil. On the suction side, the LR is confined at the first 10% of the chord, followed by a sharp MCR region. From 20% of the chord on, the response pattern does not show a significant change, and hence the TR region extends over most of the airfoil. For the pressure side, a discernible MCR is only evident for mid-frequencies around the mid-chord region. For low and high $kc$ values, the response patterns only exhibit LR and TR. Moreover, the response magnitude gradually decreases with increasing $kc$. For tripped boundary layer results, the pattern also differs from that of $\alpha = 0°$, as the tripping effect is not felt on the suction side, and the pre-transition region, which practically does not exist, is now similar to the LR for smooth flow case. However, on the pressure side, the tripping effect is evident across all $kc$ values, and the response pattern is significantly different from the suction side. The pre-transition and post-transition regions are clear for all results. For the turbulence ingestion case, the two region pattern observed at $\alpha = 0°$ evolves into a more uniform pattern over the entire airfoil on the suction across all $kc$ values. The response pattern on the pressure side differs from the suction side, with an apparent gradual increase of the energy toward the trailing edge and an overall energy decrease with an increase in the $kc$.

The detailed assessment of the results for each inflow case is as follows. Considering the results for the smooth inflow condition on the suction side, Fig. 8(a), the LR is confined to the first 5% of the chord and followed by a short MCR, where the response magnitude shows a pronounced increase. The loading reaches its maximum at $x'/c = 0.12$, and then slightly decreases. Hereafter, the loading pattern flattens and shows a relatively uniform distribution over the rest of the airfoil. The response magnitude at LR shows a pronounced reduction as $kc$ increases. However, the reduction at MCR and TR is less significant. On the pressure side, the response magnitude is significantly lower compared to the suction side across almost all $kc$ values and at all regions, except at LR for $kc = 0.73$. Moreover, the three region pattern is not persistent. At low and high $kc$ values, a stretched LR is followed by a narrow TR. At mid-frequencies, $2.21 \leq kc \leq 5.54$, at around 20% chord, the energy levels show a slight but gradual increase until the trailing edge. The results point to the fact that the suction side of the airfoil becomes more dominant on the overall airfoil response as the frequency increases.

For the tripped boundary layer case results, the leading edge exhibits similar behavior with the smooth inflow case results on the suction side of the airfoil across all the presented isolated frequencies. The response patterns across all $kc$ values suggest that the presence of the trip is not felt. Hence, instead of displaying a pre-transition region, it displays an LR region, similar to smooth inflow results. Moreover, the tripping does not significantly alter the behavior downstream, except in the vicinity of the tipping, where a slight increase in the response magnitude can be observed. The nature of the airfoil response is rather different at the pressure side of the airfoil. The presence of pre-transition resembles the results at $\alpha = 0°$, where a flat response until the tripping point is evident, after which a substantial increase in the energy is observed. Beyond this point, in the post-transition region, a slight reduction in the magnitude of the response is followed by a flat response until the trailing edge. This pattern is consistent across all $kc$ values. Furthermore, the response magnitude at the pre-transition region decreases with an increase in the $kc$ values. The results of the turbulence ingestion case, Fig. 8(c), demonstrate the impact of the impinging vortices with a dominant leading edge region at $kc = 0.73$ on both sides of the airfoil, which is followed by a decrease in the magnitude of response and a flat behavior until the trailing edge. At the trailing edge, a slight increase in the response is evident. This two region pattern is consistent with the results at $\alpha = 0°$. However, with an increase in the frequency, the response pattern varies across frequencies and between the suction and pressure sides. On the suction side, with higher $kc$ values, the energy levels decrease at the leading edge. There is no apparent transition region, and the response patterns are flat until the trailing edge, similar to patterns of smooth inflow and tripped boundary layer case. On the pressure side of the airfoil, a three region pattern is observed at low $kc$, which evolves into a two region pattern for higher $kc$ values. At $kc = 0.73$, the elevated energy levels at the leading edge decay gradually towards mid-chord. The mid-chord region displays a flat-like response pattern. At the trailing edge, a slight increase in the response magnitude is evident. Higher $kc$ values lead to a lower response magnitude at the leading edge, followed by a gradual increase of response magnitude toward the trailing edge, marking the trailing edge region as the dominant region of the airfoil.

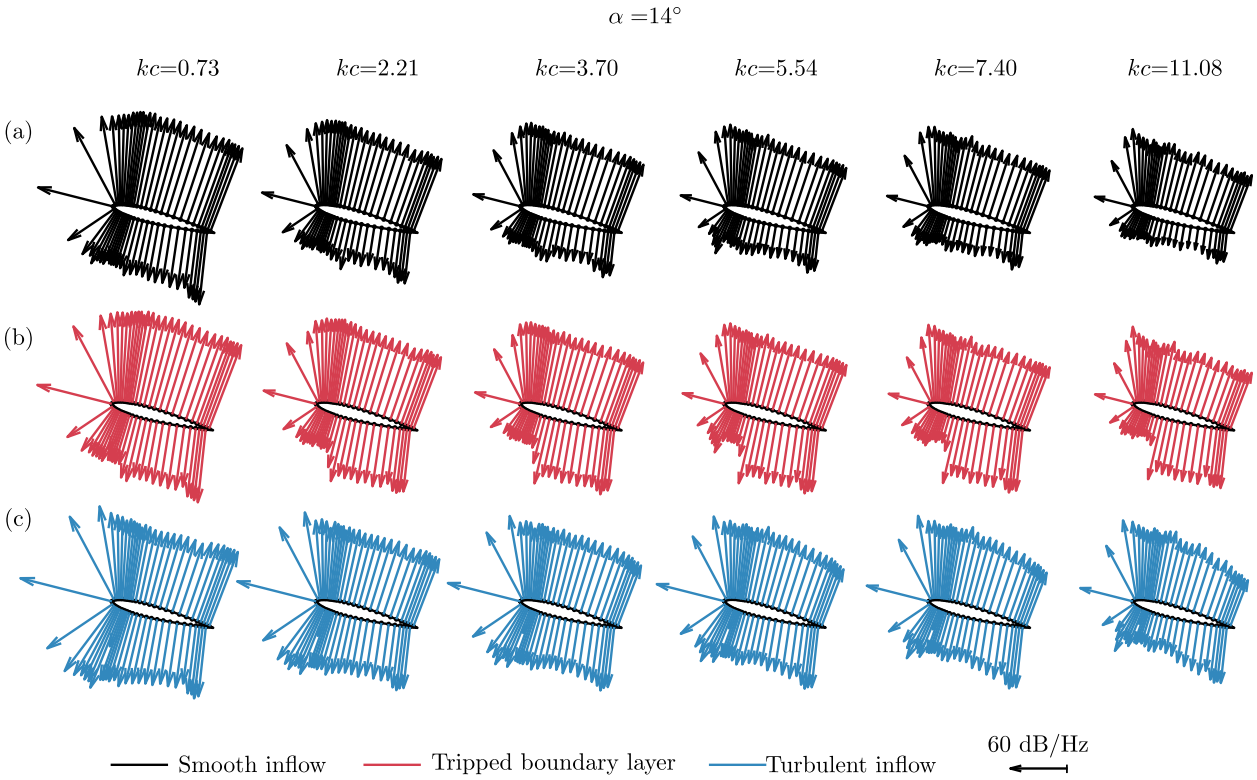


**Fig. 10 Comparison of unsteady airfoil response at angles of attack $\alpha = 14°$ for $0.73 \leq kc \leq 11.08$ under various flow conditions: (a) smooth inflow, (b) tripped boundary layer, (c) grid turbulence.**

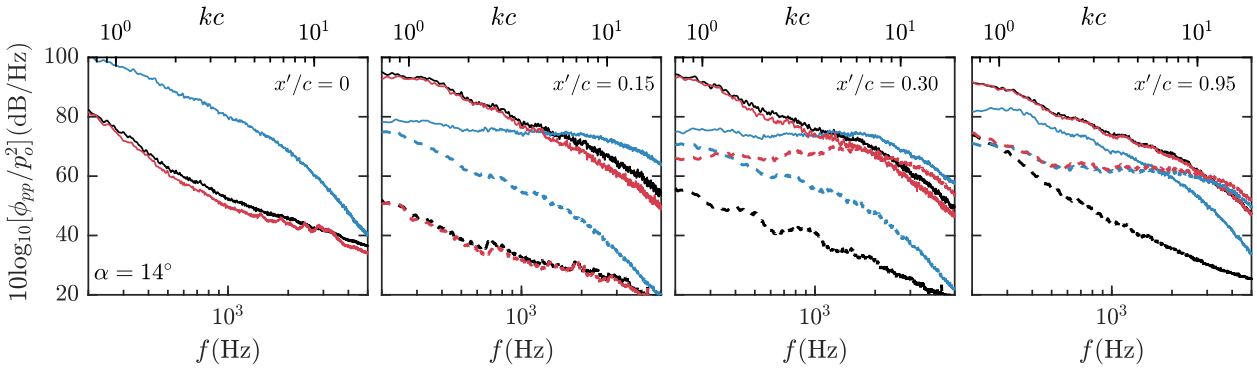


**Fig. 11 Energy spectra of the pressure fluctuations (response) for the transducers located at $x'/c = 0$, 0.15, 0.3 and 0.95 on both the pressure and suction side of the wing for different flow conditions at $\alpha = 14°$.**

The results underline two crucial outcomes. First, the loading characteristics on both sides of the airfoil are substantially different for the smooth inflow case. Moreover, the tripped boundary layer case results show an apparent difference in both the response pattern and magnitude. Considering the far-field noise prediction methods, the results suggest that the predictions based on the integration of the surface pressure fluctuations over the airfoil, such as Curle's analogy, may differ from the results calculated based on the methods which account for the trailing edge surface pressure fluctuations, such as Amiet's model. The second important point is that tripping the boundary layer on both sides of the

airfoil in the experiments generates a response pattern which may not be a true indicator of real-life experience, as the pattern on the pressure side of the airfoil is significantly different for smooth inflow and tripped boundary layer case.

It is clear from these discussions that the effect of the inflow condition on the airfoil response is rich in complexity. The footprints of T-S waves are present at the leading edge for the smooth inflow case at$\alpha = 6^\circ$, as displayed in Fig. 9. These instabilities vanish over the suction side of the airfoil. Moreover, the suction side response is uniform over the airfoil across most of the frequency range, a common feature shared with the turbulent inflow and tripped boundary layer cases. Conversely, T-S waves persist over the entire airfoil on the pressure side of the airfoil. The results also indicate that the energy level of the T-S waves increases toward the trailing edge. The energy spectra of the tripped boundary layer case at the leading edge corroborate the pattern similarity with smooth inflow condition. The difference between the two cases becomes evident around the frequency of T-S waves. The energy spectrum at $x'/c = 0.15$ suggests the lack of tripping effect with a significant difference in the spectra between smooth inflow and tripped cases. The tripping reflects its effect, i.e., pre and post transition region, on the spectra at $x'/c = 0.3$. It is worth recalling that the results in Fig. 8 suggest that the tripping is effective on the pressure side only, yet the energy spectra on both sides of the airfoil are similar. The results also clearly indicate that the enhanced response levels at the leading edge for the turbulent inflow case weaken towards the trailing edge, where all the cases lead a similar response over the airfoil, except the pressure side of the smooth inflow case. Considering all the results together, one can deduce that the response patterns and magnitude on the suction side of the airfoil are less affected by the flow condition. Conversely, the tripping or incoming turbulence seems to affect both the response patterns and the response magnitude on the pressure side.

At sufficiently high angle of attack, $\alpha = 14^\circ$, where the flow has started to separate for the smooth inflow case and the tripped boundary layer case according to steady pressure distribution results, airfoil response patterns show a significant change, as displayed in Fig. 10. The response pattern for smooth inflow conditions evolved into a two region pattern on the suction side, with a uniform LR confined to the first 20% of the chord, followed by a flat response over the entire airfoil without an apparent transition region (MCR). The response magnitude gradually decays as the $kc$ increases. The response on the pressure side of the airfoil resembles the results at $\alpha = 6^\circ$ with a two region pattern, and similar to the suction side, the response magnitude decreases as the $kc$ increases. The tripped boundary layer results are similar to the smooth inflow case results for low $kc$ on the suction side. The tripping does not affect the airfoil response patterns across all $kc$ values. On the pressure side, however, the tripping effect is evident starting from $kc = 0.73$, and both pre-transition and post-transition regions are present. Moreover, the tripped boundary layer shows elevated energy levels at high $kc$ compared to the smooth inflow case results on the pressure side. The airfoil surface patterns for the turbulence interaction case show marked differences compared to the smooth inflow and tripped boundary layer cases. The response at the leading edge at low $kc$ is significantly higher compared to the other cases. The elevated energy level at the leading edge decreases as $kc$ increases on both sides of the airfoil. Furthermore, At high $kc$ values, the response magnitude increases toward the trailing edge.

A more detailed assessment for each inflow case is as follows. For the smooth inflow case, Fig. 10, after a short LR, where the magnitude of the response slightly increases within the first 15% of the chord, the response evolves into a a flat pattern until the trailing edge across all $kc$ values. It is worth mentioning that the overall magnitude of the response gradually decreases as the $kc$ increases. Furthermore, the decrease at LR is more prominent compared to the rest of the airfoil. The pressure side of the airfoil depicts a slightly different picture than the suction side. Firstly, for all $kc$ values, the response magnitude is lower compared to the suction side results. Moreover, across all $kc$ values, the results at the trailing edge region show a slight increase. Secondly, for $kc \leq 3.70$, the energy levels increase toward trailing edge. For higher $kc$ vales, the response is relatively flat over the entire pressure side.

For the tripped boundary layer case, at $kc = 0.73$, the effect of tripping is not felt on the suction side. Moreover, a slight increase in the response magnitude is evident on the pressure side. However, the overall pattern is similar to the smooth inflow pattern. With increasing $kc$, the magnitude of the response at the leading edge of the suction side reduces gradually. The level of reduction is high at the first few percent of the chord compared to the rest. From $kc = 2.21$ on, the tripping effect is observable. The apparent pre-transition region on the pressure side weakens with an increase in $kc$. The post-transition region displays a flat-like pattern over the rest of the airfoil. It is worth noting that the asymmetrical airfoil responses and the significant magnitude differences between the smooth inflow case and tripped boundary layer case imply that the development of flow is different markedly, which reflects on both the steady and unsteady response. Moreover, the magnitude difference on the pressure side of the airfoil t high frequencies should also be considered a point of discrepancy when tripping is used to energize the flow with an assumption of replicating the actual behavior. These results suggest that the flow structures generated by the tripping for experimental purposes may not produce the flow structures encountered in real scenarios.

In the presence of the turbulent inflow, Fig. 10(c), the results show that the leading edge remains as the dominant region for low $kc$ values on both sides of the airfoil. An increase in the frequency leads to a decrease in the magnitude of the response over the entire airfoil. However, the leading edge remains as the location with the highest magnitude of response. On the suction side, the flat-like response over the airfoil at low $kc$ changes for $kc \geq 3.70$, where a decay in magnitude becomes apparent. The decay and hence the difference in response magnitude between the leading edge and trailing edge reaches its peak at the highest $kc$ value. On the pressure side, the elevated response magnitudes at the leading edge is followed by a gradual, yet slow decay until the trailing edge region. where a prominent increase is evident at $kc = 0.73$. Increase in the $kc$ evolves this patterns into a flat-like behavior for mid-frequencies. At higher $kc$ values, $kc \geq 7.40$, an increase of the response is evident toward trailing edge.

Energy spectra at the selected transducer locations for the three flow cases are presented in Fig. 11 and display a few important points to underline. At the leading edge, the smooth inflow and tripped boundary layer cases exhibit similar energy spectra, whereas the energy spectra for the turbulent inflow case differs substantially over an extensive range, except at high frequencies. Further downstream, the footprints of T-S waves seem to be eliminated for the smooth

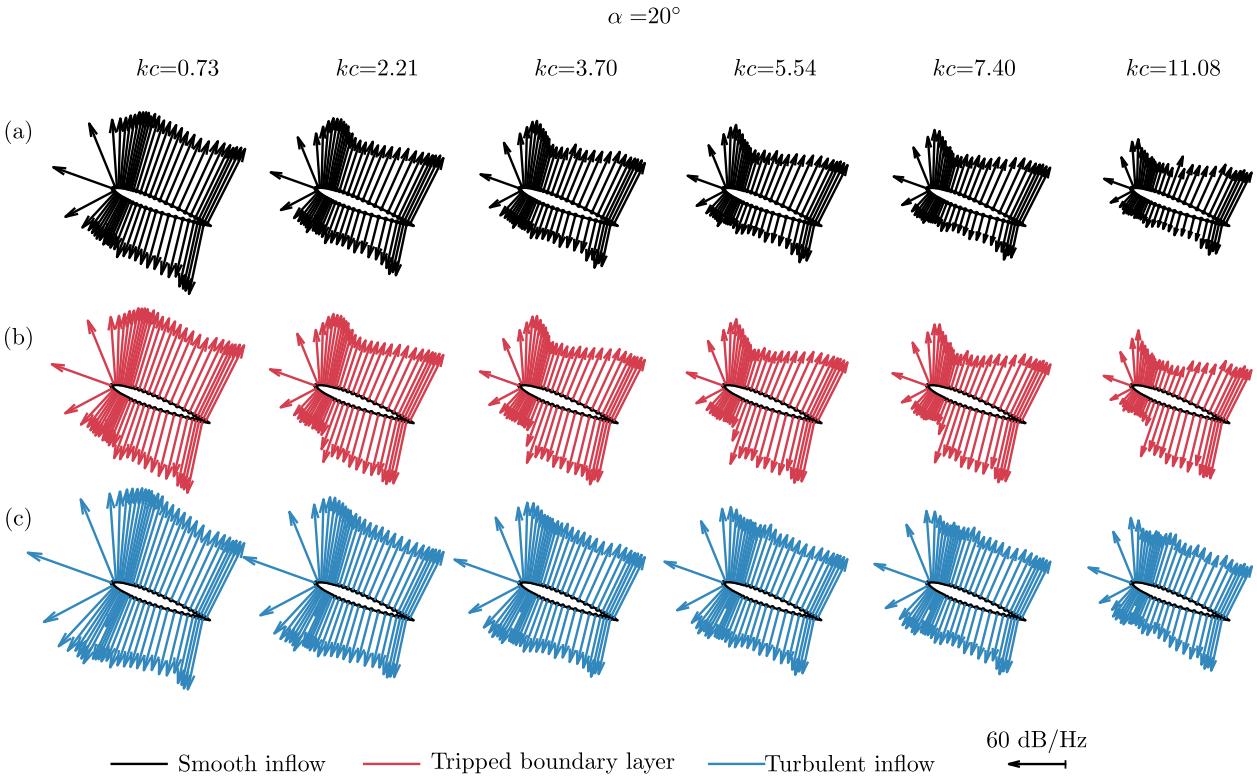


**Fig. 12 Comparison of unsteady airfoil response at angles of attack $\alpha = 20°$ for $0.73 \leq kc \leq 11.08$ under various flow conditions: (a) smooth inflow, (b) tripped boundary layer, (c) grid turbulence.**

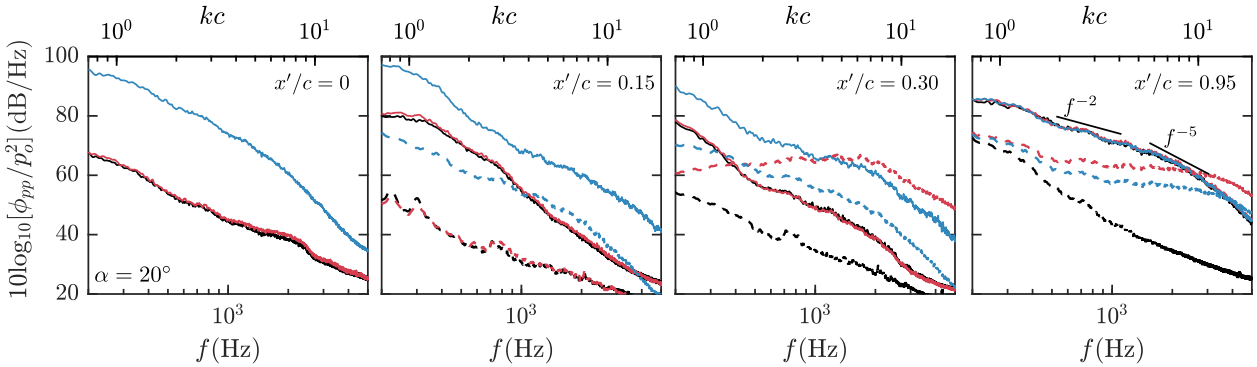


**Fig. 13 Energy spectra of the pressure fluctuations (response) for the transducers located at $x'/c = 0$, 0.15, 0.3 and 0.95 on both the pressure and suction side of the wing for different flow conditions at $\alpha = 20°$.**

inflow case results. At around the mid-chord region, the suction side of the airfoil exhibits similar energy spectra for the smooth inflow case and the tripped boundary layer case, which is indicative of separated flow with a decay rate of $f^{-5}$ over the entire frequency range. However, the results of the turbulent inflow case show a typically attached flow spectrum. At the trailing edge, the energy spectra for the smooth inflow case and tripped boundary layer case exhibits similar behavior, and the spectra of the turbulent inflow case evolved into a similar pattern with other cases with slightly lower energy levels.

Figures 12 and 13 present the results of the airfoil response at $\alpha = 20°$, where the steady pressure coefficient results in Fig. 4 show a flat response, indicating that airfoil is experiencing a deep stall for all three cases. Surprisingly, at this angle of attack, the response patterns are as rich as $\alpha = 0°$. For smooth inflow case, the three region pattern becomes evident on the suction side, with a distinct pattern as opposed to the previous three region patterns observed in lower angles of attack. The pattern becomes more discernible at higher $kc$ values. The leading edge region (LR) is followed by a sharp increasing-decreasing transition region (MCR), which finally turns into a gradually increasing response until the trailing edge (TR). The overall magnitude of the response decreases as the $kc$ increases, consistent with the previously displayed results. The pressure side pattern for the smooth inflow case is similar to the results of the $\alpha = 14°$, where a gradual increase toward the trailing edge is evident up to $kc = 3.70$. For $kc > 3.70$, the response pattern shows a monotonic behavior from leading edge to trailing edge. The tripped case results show that the tripping has no effect on the airfoil response on the suction side when the airfoil is stalled, and the response pattern is remarkably similar with smooth inflow conditions. On the pressure side, the presence of tripping is felt for higher $kc$ values, and two region pattern, i.e., pre-transition and post-transition, is apparent. For the turbulence ingestion case, a two region behavior is evident for low $kc$ values, which then evolves into a flat response over the entire airfoil at higher $kc$ values in the suction side of the airfoil. A two region behavior is evident on the pressure side with a stretching leading edge effect (impact region) and a short trailing edge region. This pattern slightly changes into a pattern with gradually increasing response magnitude at high $kc$ values.

In order to gain a better understanding of the patterns, a more detailed assessment may be helpful. The results show a strong dependency of response pattern to $kc$ for the smooth inflow case. At the lowest frequency, $kc = 0.73$, the suction side of the airfoil exhibits all three regions, LR, MCR and TR. The LR is confined in a narrow region, which is followed by a stretched MCR. The MCR shows an increasing-decreasing region, which is then followed by a flat-like response until the trailing edge. The response in TR shows a slight increase compared to the flat-like region in the MCR. Furthermore, at higher frequencies, the response patterns change drastically. For $2.21 \leq kc \leq 11.08$, the MCR dominates the response with a significantly higher magnitudes, which is followed by sharp decay before the mid-chord region. From this location on, until the trailing edge, the response magnitude increases gradually. Although the response magnitude decreases as the $kc$ increases, the pattern remains similar on the suction side. The response on the pressure side displays a similar pattern across all $kc$ values, with a decrease in the magnitude as the $kc$ increases. The magnitude of the response shows almost a flat behavior over the entire airfoil with a slight increase at the trailing edge. The results of the tripped boundary layer case, Fig. 12(b), shows similar behavior to the results of the smooth inflow case at $kc = 0.73$, as observed in the results for $\alpha = 14°$. For higher $kc$ values, the results on the suction side follow a similar pattern with the smooth inflow case with a higher magnitude in response. On the pressure side of the airfoil, the effect of the tripping is prominent for $kc \leq 2.21$. More interestingly, the response on the pressure side is relatively flat until the trailing edge and almost always higher in magnitude compared to the response magnitude on the

suction side (except for the pre-transition region). For the turbulent inflow case, the response at the leading edge mimics the pattern of the previous cases with a higher response magnitude at $kc = 0.73$, except for the impact region, where an elevated level of response magnitude is evident. As the frequency increases, the response pattern on the suction side of the airfoil becomes flat until the trailing edge as opposed to the decreasing-increasing pattern observed for the smooth inflow case and tripped boundary layer case. The pressure side response pattern is similar to the suction side with lower magnitudes, and displays a slight increase at the trailing edge. The results and response pattern at $\alpha = 20°$ display the prominent difference between the smooth and tripped flow cases. The detailed map of the significant difference on both sides of the wing for all cases, both pattern wise and energy level wise, may also help both to improve and to understand the recent models developed for stall noise predictions in literature [25, 26, 54] after Amiet's model and Curle's analogy.

The energy spectra at selected transducers in Fig. 13 also corroborates the asymmetrical nature of the airfoil response for all inflow cases, as well as the difference among each case. For the transducer located at the leading edge, the significant energy difference between the turbulent inflow and other cases is consistent with the results of other angles of attack and highlights the difference generated by the incoming turbulent structures at $x'/c = 0$. At $x'/c = 0.15$, the spectrum displays the similarity of the smooth inflow case and the tripped boundary layer case. Moreover, the spectrum for turbulence ingestion case displays a prominent increase compared to the smooth inflow and tripped boundary layer case results. The spectrum at $x'/c = 0.3$, where the effect of tripping is evident on the pressure side (Fig. 12(b)), clearly displays how the energy content differs compared to the smooth inflow case. At the trailing edge, the spectra is similar for all three cases, and decays with $f^{-2}$ for $kc < 3.70$ and $f^{-5}$ for $kc > 5.54$. On the pressure side, both the tripped boundary layer case and the turbulence ingestion case show a similar spectrum. The spectra of the smooth inflow case deviate from the other cases in terms of magnitude and decay pattern.

## V. Conclusion

The nature behind the unsteady airfoil response is rich and still requires a systematic and collective effort to understand the underpinning physical phenomenon for a broad range of application field, including aeroacoustics, aerodynamics and aeroelasticity. The experimental studies performed to understand this phenomenon and provide data sets for prediction methods vary in terms of the inputs. This investigation aims at providing a detailed map of the unsteady airfoil response under different conditions. The experiments were performed with a NACA0012 airfoil for a broad range of angles of attack ($0° \leq \alpha \leq 20°$). Moreover, the experiments were performed for three inflow conditions, i.e., smooth inflow, turbulence ingestion, and a smooth inflow with a tripped boundary layer, to reveal the surface pressure fluctuation patterns over the entire airfoil. The results are presented in terms of mean pressure coefficients, root mean square surface pressure coefficient, unsteady airfoil response patterns at isolated frequencies, and frequency-energy content at selected transducer locations.

Non-dimensional pressure coefficient ($C_p$) distributions show that smooth inflow and tripped boundary layer cases

have similar patterns at both pre- and post-stall conditions. Turbulence ingestion delays stall, i.e., $C_p$ results display elevated values at $\alpha = 14°$, where both smooth inflow and tripped boundary layer case results show a flat-like behavior. Although the mean quantities of $C_p$ and $C_{p,rms}$ do not vary significantly between smooth inflow and tripped boundary layer cases, the unsteady airfoil response results suggest a pronounced difference between the two cases. The unsteady airfoil response patterns display rich patterns varying with inflow conditions and angles of attack. It is worth noting that the response pattern over the airfoil is asymmetrical for $\alpha > 0°$, and with increasing angles of attack, the initial patterns observed at $\alpha = 0°$ evolve. The results display that the transition of the response around the tripping point is gradual at lower $kc$ values and sharper at higher $kc$ values. Moreover, the results suggest that tripping is primarily affecting the pressure side of the airfoil for $\alpha > 0°$ and increasing the response magnitude markedly compared to the smooth inflow results. Comparison of smooth inflow and tripped boundary layer case results indicate that tripping the boundary layer to accelerate the transition to turbulent flow in experiments may provide a statistically relevant flow. However, since the boundary layer development is not natural, the behavior of the structures and energy content in the boundary layer may not be similar to a flow with a natural transition. This may raise questions about the accurate representation of small-scale experiments for full-scale products, such as wind turbine blades, especially for quantities in the frequency domain. The response associated with the turbulence ingestion case has a strong impact region at the leading edge for almost all cases with the highest response magnitude for all angles of attack and across most $kc$ values. The elevated energy region is then followed by an adjustment (decreasing-increasing recovery region) where it reaches a flat-like behavior until the trailing edge on the suction side of the airfoil. On the pressure side, after the impact region, the energy levels decrease and remain flat-like pattern for medium $kc$ values and a gradually increasing pattern toward the trailing edge for higher $kc$ values.

## Acknowledgments

The first author (A.C.) would like to acknowledge the financial support of EPSRC via grant number EP/S013024/1 between 01.06.2020 - 30.11.2021 at the University of Bristol. The second author (L.B.) would like to acknowledge the financial support of Embraer S.A. and EPSRC Doctoral training partnership award.

## References


[1] ACARE, "Flightpath 2050 - Europe's Vision for Aviation," *Publications Office of the European Union*, 2011, p. Luxembourg.

[2] WHO, "ENVIRONMENTAL NOISE GUIDELINES for the European Region," *World Health Organization Regional Office for Europe*, 2018, p. Denmark.

[3] Roddle, D., "Wind-tunnel investigation of surface-pressure fluctuations associated with aircraft buffet," *13th Aerospace Sciences Meeting, Pasadena, CA*, 1975. https://doi.org/10.2514/6.1975-67.

[4] Zhao, X., and Ai, B., "Predicting the Structural Response Induced by Turbulent Boundary Layer in Wind Tunnel," *AIAA Journal*, Vol. 55, No. 4, 2017, pp. 1221–1229. https://doi.org/10.2514/1.J055576.

[5] Maury, C., Gardonio, P., and Elliott, S., "A Wave Number Approach to Modelling the Response of a Randomly Excited Panel, Part I: General Theory," *Journal of Sound and Vibration*, Vol. 252, No. 1, 2002, pp. 83–113.

[6] Bonness, W. K., Fahnline, J. B., Lysak, P. D., and Shepherd, M. R., "Modal forcing functions for structural vibration from turbulent boundary layer flow," *Journal of Sound and Vibration*, Vol. 395, 2017, pp. 224–239.

[7] Curle, N., and Lighthill, M. J., "The influence of solid boundaries upon aerodynamic sound," *Proceedings of the Royal Society of London. Series A. Mathematical and Physical Sciences*, Vol. 231, No. 1187, 1955, pp. 505–514. https://doi.org/10.1098/rspa.1955.0191.

[8] Sears, W. R., "Some Aspects of Non-Stationary Airfoil Theory and Its Practical Application," *Journal of the Aeronautical Sciences*, Vol. 8, No. 3, 1941, pp. 104–108. https://doi.org/10.2514/8.10655.

[9] Amiet, R., "Acoustic radiation from an airfoil in a turbulent stream," *Journal of Sound and Vibration*, Vol. 41, No. 4, 1975, pp. 407 – 420. https://doi.org/10.1016/S0022-460X(75)80105-2.

[10] Theodorsen, T., "General Theory of Aerodynamic Instability and the Mechanism of Flutter," Tech. rep., National Aeronautics of Space Administration, Office of Management, 1935. NACA Technical Report No. 496.

[11] von Karman, T., and Sears, W. R., "Airfoil Theory for Non-Uniform Motion," *Journal of the Aeronautical Sciences*, Vol. 5, No. 10, 1938, pp. 379–390. https://doi.org/10.2514/8.674.

[12] Atassi, H. M., "The Sears problem for a lifting airfoil revisited - new results," *Journal of Fluid Mechanics*, Vol. 141, 1984, p. 109–122. https://doi.org/10.1017/S0022112084000768.

[13] Brooks, T., Pope, D., and Marcolini, M., "Airfoil self-noise and prediction," Tech. rep., National Aeronautics of Space Administration, Office of Management, 1989. Rep. No. NASA-RP-1218.

[14] Howe, M., "A review of the theory of trailing edge noise," *Journal of Sound and Vibration*, Vol. 61, No. 3, 1978, pp. 437 – 465. https://doi.org/10.1016/0022-460X(78)90391-7.

[15] Ffowcs Williams, J. E., and Hawkings, D. L., "Sound generation by turbulence and surfaces in arbitrary motion," *Philosophical Transactions of the Royal Society of London. Series A, Mathematical and Physical Sciences*, Vol. 264, No. 1151, 1969, pp. 321–342. https://doi.org/10.1098/rsta.1969.0031.

[16] Amiet, R., "Noise due to turbulent flow past a trailing edge," *Journal of Sound and Vibration*, Vol. 47, No. 3, 1976, pp. 387 – 393. https://doi.org/10.1016/0022-460X(76)90948-2.

[17] Chase, D. M., "Noise Radiated from an Edge in Turbulent Flow," *AIAA Journal*, Vol. 13, No. 8, 1975, pp. 1041–1047. https://doi.org/10.2514/3.60502.

[18] Howe, M., "Unsteady lift and sound produced by an airfoil in a turbulent boundary layer," *Journal of Fluids and Structures*, Vol. 15, No. 2, 2001, pp. 207 – 225. https://doi.org/10.1006/jfls.2000.0335.

[19] Oerlemans, S., and Migliore, P., *Aeroacoustic Wind Tunnel Tests of Wind Turbine Airfoils*, chapter and pages. https://doi.org/10.2514/6.2004-3042.

[20] Moreau, S., and Roger, M., *Effect of Angle of Attack and Airfoil Shape on Turbulence-Interaction Noise*, chapter and pages. https://doi.org/10.2514/6.2005-2973.

[21] Mckeough, P., and Graham, J., "The Effect of Mean Loading on the Fluctuating Loads Induced on Aerofoils by a Turbulent Stream," *Aeronautical Quarterly*, Vol. 31, No. 1, 1980, p. 56–69. https://doi.org/10.1017/S0001925900008829.

[22] Mish, P. F., and Devenport, W. J., "An experimental investigation of unsteady surface pressure on an airfoil in turbulence—Part 1: Effects of mean loading," *Journal of Sound and Vibration*, Vol. 296, No. 3, 2006, pp. 417 – 446.

[23] Mish, P. F., and Devenport, W. J., "An experimental investigation of unsteady surface pressure on an airfoil in turbulence—Part 2: Sources and prediction of mean loading effects," *Journal of Sound and Vibration*, Vol. 296, No. 3, 2006, pp. 447 – 460.

[24] Devenport, W. J., Staubs, J. K., and Glegg, S. A., "Sound radiation from real airfoils in turbulence," *Journal of Sound and Vibration*, Vol. 329, No. 17, 2010, pp. 3470 – 3483.

[25] Moreau, S., Roger, M., and Christophe, J., "Flow Features and Self-Noise of Airfoils Near Stall or in Stall," *15th AIAA/CEAS Aeroacoustics Conference (30th AIAA Aeroacoustics Conference) - AIAA 2009-3198*, Miami, FL, 2009. https://doi.org/10.2514/6.2009-3198.

[26] Bertagnolio, F., Madsen, H. A., Fischer, A., and Bak, C., "A semi-empirical airfoil stall noise model based on surface pressure measurements," *Journal of Sound and Vibration*, Vol. 387, 2017, pp. 127–162. https://doi.org/https://doi.org/10.1016/j.jsv.2016.09.033.

[27] Mayer, Y. D., Zang, B., and Azarpeyvand, M., "Aeroacoustic investigation of an oscillating airfoil in the pre- and post-stall regime," *Aerospace Science and Technology*, Vol. 103, 2020, p. 105880. https://doi.org/10.1016/j.ast.2020.105880.

[28] Zang, B., Mayer, Y. D., and Azarpeyvand, M., "Experimental Investigation of Near-Field Aeroacoustic Characteristics of a Pre- and Post-Stall NACA 65-410 Airfoil," *Journal of Aerospace Engineering*, Vol. 34, No. 6, 2021, p. 04021080. https://doi.org/10.1061/(ASCE)AS.1943-5525.0001318.

[29] Amiet, R. K., "High frequency thin-airfoil theory for subsonic flow," *AIAA Journal*, Vol. 14, No. 8, 1976, pp. 1076–1082.

[30] Santana, L. D., Schram, C., and Desmet, W., "Low-frequency extension of Amiets theory for compact airfoil noise predictions," *Journal of Sound and Vibration*, Vol. 372, 2016, pp. 342–356.

[31] Miotto, R. F., Wolf, W. R., and de Santana, L. D., "Numerical computation of aeroacoustic transfer functions for realistic airfoils," *Journal of Sound and Vibration*, Vol. 407, 2017, pp. 253 – 270.

[32] Santana, L. D., Christophe, J., Schram, C., and Desmet, W., "A Rapid Distortion Theory modified turbulence spectra for semi-analytical airfoil noise prediction," *Journal of Sound and Vibration*, Vol. 383, 2016, pp. 349 – 363.

[33] Amiet, R., and Sears, W. R., "The aerodynamic noise of small-perturbation subsonic flows," *Journal of Fluid Mechanics*, Vol. 44, No. 2, 1970, p. 227–235. https://doi.org/10.1017/S0022112070001805.

[34] Goldstein, M. E., and Atassi, H., "A complete second-order theory for the unsteady flow about an airfoil due to a periodic gust," *Journal of Fluid Mechanics*, Vol. 74, No. 4, 1976, p. 741–765. https://doi.org/10.1017/S0022112076002036.

[35] Glegg, S. A. L., "Sound radiation from an airfoil encountering an oblique gust in its plane of motion," *AIAA Journal*, Vol. 27, No. 12, 1989, pp. 1820–1822. https://doi.org/10.2514/3.10340.

[36] Vemuri, S. S., Liu, X., Zang, B., and Azarpeyvand, M., "On the use of leading-edge serrations for noise control in a tandem airfoil configuration," *Physics of Fluids*, Vol. 32, No. 7, 2020, p. 077102. https://doi.org/10.1063/5.0012958, URL https://doi.org/10.1063/5.0012958.

[37] Kamliya Jawahar, H., Showkat Ali, S. A., and Azarpeyvand, M., "Serrated slat cusp for high-lift device noise reduction," *Physics of Fluids*, Vol. 33, No. 1, 2021, p. 015107. https://doi.org/10.1063/5.0035178, URL https://doi.org/10.1063/5.0035178.

[38] Kamliya Jawahar, H., Meloni, S., Camussi, R., and Azarpeyvand, M., "Intermittent and stochastic characteristics of slat tones," *Physics of Fluids*, Vol. 33, No. 2, 2021, p. 025120. https://doi.org/10.1063/5.0033827, URL https://doi.org/10.1063/5.0033827.

[39] Chaitanya, P., and Joseph, P., "Slitted leading edge profiles for the reduction of turbulence-aerofoil interaction noise," *The Journal of the Acoustical Society of America*, Vol. 143, No. 6, 2018, pp. 3494–3504. https://doi.org/10.1121/1.5040972.

[40] Shah, Y., and Yarusevych, S., "Streamwise evolution of drag reduced turbulent boundary layer with polymer solutions," *Physics of Fluids*, Vol. 32, No. 6, 2020, p. 065108. https://doi.org/10.1063/5.0009371.

[41] Traub, L. W., "Experimental Investigation of the Effect of Trip Strips at Low Reynolds Number," *Journal of Aircraft*, Vol. 48, No. 5, 2011, pp. 1776–1784. https://doi.org/10.2514/1.C031375.

[42] Sreejith, B. K., Sathyabhama, A., and Kumar, S. S., "Comparative study on the aerodynamic performance of airfoil with boundary layer trip of various geometrical shapes," *Journal of Physics: Conference Series*, Vol. 1854, No. 1, 2021, p. 012003. https://doi.org/10.1088/1742-6596/1854/1/012003.

[43] Braslow, A. L., and Knox, E. C., "Simplified Method for Determination of Critical Height of Distributed Roughness Particles for Boundary-layer Transition at Mach Numbers from 0 to 5," Tech. rep., Langley Aeronautical Laboratory, NACA, 1958. Rep. No. NACA-TN-4363.

[44] Mayer, Y. D., Jawahar, H. K., Szőke, M., Ali, S. A. S., and Azarpeyvand, M., "Design and performance of an aeroacoustic wind tunnel facility at the University of Bristol," *Applied Acoustics*, Vol. 155, 2019, pp. 358 – 370. https://doi.org/10.1016/j.apacoust.2019.06.005.

[45] Welch, P., "The use of fast Fourier transform for the estimation of power spectra: A method based on time averaging over short, modified periodograms," *IEEE Transactions on Audio and Electroacoustics*, Vol. 15, No. 2, 1967, pp. 70–73.

[46] Bowen, L., Celik, A., Azarpeyvand, M., and da Silva, C. R. I., "Grid Generated Turbulence for Aeroacoustic Facility," *AIAA Journal*, Vol. 0, No. 0, 0, pp. 1–15. https://doi.org/10.2514/1.J060851.

[47] Garcia-Sagrado, A., and Hynes, T., "Wall-Pressure Sources Near an Airfoil Trailing Edge Under Separated Laminar Boundary Layers," *AIAA Journal*, Vol. 49, No. 9, 2011, pp. 1841–1856. https://doi.org/10.2514/1.J050477.

[48] Ye, Q., Avallone, F., Ragni, D., Choudhari, M., and Casalino, D., "Effect of Surface Roughness Geometry on Boundary-Layer Transition and Far-Field Noise," *AIAA Journal*, Vol. 59, No. 7, 2021, pp. 2396–2408. https://doi.org/10.2514/1.J059335.

[49] Zang, B., Mayer, Y., and Azarpeyvand, M., "An Experimental Investigation on the Mechanism of Tollmien-Schlichting Waves for a NACA 0012 Aerofoil," *25th AIAA/CEAS Aeroacoustics Conference - AIAA 2019-2609*, Delft, the Netherlands, 2019. https://doi.org/10.2514/6.2019-2609.

[50] Celik, A., Bowen, J. L., and Azarpeyvand, M., "Effect of trailing-edge bevel on the aeroacoustics of a flat-plate," *Physics of Fluids*, Vol. 32, No. 10, 2020, p. 105116. https://doi.org/10.1063/5.0024248.

[51] Celik, A., Mayer, Y. D., and Azarpeyvand, M., "On the aeroacoustic characterization of a robust trailing-edge serration," *Physics of Fluids*, Vol. 33, No. 7, 2021, p. 075120. https://doi.org/10.1063/5.0054767.

[52] Goody, M., "Empirical Spectral Model of Surface Pressure Fluctuations," *AIAA Journal*, Vol. 42, No. 9, 2004, pp. 1788–1794. https://doi.org/10.2514/1.9433.

[53] Gravante, S. P., Naguib, A. M., Wark, C. E., and Nagib, H. M., "Characterization of the Pressure Fluctuations Under a Fully Developed Turbulent Boundary Layer," *AIAA Journal*, Vol. 36, No. 10, 1998, pp. 1808–1816. https://doi.org/10.2514/2.296.

[54] Fischer, A., Madsen, H. A., and Bertagnolio, F., "Experimental Investigation of the Surface Pressure Field for Prediction of Trailing Edge Noise of Wind Turbine Aero Foils," *International Journal of Aeroacoustics*, Vol. 14, No. 5-6, 2015, pp. 767–809. https://doi.org/10.1260/1475-472X.14.5-6.767.